DOI: https://doi.org/10.62985/j.huit_ojs.vol26.no2E.394

ANALYSIS OF FLUX BARRIER EFFECTS ON MAGNETIC FLUX DISTRIBUTION AND TORQUE CHARACTERISTICS IN SPOKE-TYPE INTERIOR PERMANENT MAGNET SYNCHRONOUS MOTORS

Anh Thanh Huynh[1*], Viet-Vu Do[2], Minh-Hoc Duong Le[3,4], and Min-Fu Hsieh[3]

[1]*Power Electronics, Machines and Control Research Institute,*
University of Nottingham, Nottingham, United Kingdom
[2]*University of Technology and Education - The University of Danang, Danang, Vietnam*
[3]*Department of Electrical Engineering, National Cheng Kung University, Tainan, Taiwan*
[4]*Electric Motor Technology Research Center,*
National Cheng Kung University, Tainan, Taiwan
*Email: *anh.huynh@nottingham.ac.uk*

Received: 15 December 2025; Revised: 3 January 2026; Accepted: 14 April 2026

ABSTRACT

This paper investigates how multiple flux barriers (FBs) affect the magnetic flux distribution and torque performance of Spoke-Type Interior Permanent Magnet Synchronous (SIPM) motors for electric vehicle (EV) applications. A 5-kW conventional SIPM motor serves as the baseline for comparison. The study first explores how multiple FBs influence the magnetic flux density, air-gap flux density, cogging torque, and inductance characteristics (L_d and L_q) under both no-load and load conditions. Applying a positive I_d current lead to flux enhancement, increasing the effective PM flux density in the rotor. This results in higher torque output and reduces the risk of irreversible magnet demagnetization. Integrating multiple FBs into the rotor core yields significant performance improvements over a wide speed range. All findings are validated through finite-element method (FEM) simulations.

Keywords: Flux Intensifying (FI), Permanent Magnet, Multiple Flux Barriers, Spoke-type.

1. INTRODUCTION

Recent years have seen growing research interest in traction machines for electric vehicles (EVs), driven by the rapid expansion of the EV market and increasingly stringent requirements for power density, efficiency, reliability, and operating speed range [1]. Among various candidates, interior permanent magnet synchronous machines (IPMSMs) have emerged as a leading solution for EV traction due to their high torque and power density, low torque ripple, and wide constant power speed range (CPSR), a critical requirement for high-performance EV propulsion systems [2].

For conventional IPMSMs with U-, V-, or delta-shaped permanent magnet (PM) configurations, extending the operating speed range beyond the base speed is typically achieved through field-weakening (FW) control. This is accomplished by injecting a negative *d*-axis current ($i_d < 0$) to reduce the effective air-gap flux and meet the inverter voltage constraint [3]. While FW control effectively expands the speed range, it inevitably increases copper losses and imposes significant demagnetizing stress on the PMs, particularly at high speeds and high currents.

Compared with conventional IPMSMs, spoke-type interior permanent magnet (SIPM) motors inherently exhibit a strong flux-concentration (FC) effect, resulting from the radial orientation of the PMs and the associated magnetic circuit configuration. This FC effect enables higher air-gap flux density and torque density with reduced PM volume, making SIPM motors particularly attractive for EV traction applications that require compact size and high output capability [3]. In addition, SIPM motors generally offer a wider CPSR than conventional IPMSMs due to their enhanced saliency and flux-control capability. However, the pronounced FC effect in SIPM motors also results in a large PM flux linkage. As a result, a relatively large negative *d*-axis current is required during FW operation at high speed to suppress the air-gap flux. This significantly increases demagnetizing stress on the PMs and raises the risk of irreversible demagnetization, especially under high-speed, overload, or fault conditions [3]-[6]. Therefore, a fundamental tradeoff exists in SIPM motors between achieving high torque density through flux concentration and ensuring robust resistance to demagnetization during high-speed operation. Addressing this tradeoff while maintaining high torque density and wide-speed capability has become a key research challenge.

To overcome these limitations, the flux-intensifying (FI) operating principle has been introduced and applied to SIPM motors. Under the FI principle, the motor operates with a positive *d*-axis current ($i_d > 0$) below the base speed to reinforce the PM flux and enhance torque production, while requiring only a small negative *d*-axis current above the base speed for FW operation [7]. The FI operation relies on two essential characteristics: (i) rotor saliency condition, with *d*-axis inductance exceeding *q*-axis inductance ($L_d > L_q$), and (ii) the intentional use of a positive *d*-axis current, referred to as the FI current, rather than a negative FW current. Unlike conventional FW control, the FI current assists the PM flux rather than opposing it, enabling higher torque under maximum torque per ampere (MTPA) operation and substantially reducing the risk of PM demagnetization. As the operating speed increases and the inverter voltage limit is reached, the current vector is progressively advanced, reducing the *q*-axis current (i_q) and transitioning the *d*-axis current from positive to a small negative value. This transition enables effective FW capability while keeping the magnitude of negative i_d lower than in conventional IPMSMs [8]. Furthermore, the condition $L_d > L_q$ preserves rotor saliency and can even enhance it under load, which is advantageous for sensorless control strategies that rely on saliency-based position estimation [7], [9], [10].

The FI effect can be achieved by introducing multiple flux barrier (FB) elements into the rotor structure to reshape the magnetic circuit and adjust the inductance characteristics [10]. In particular, appropriately placed FBs can effectively reduce L_q while maintaining or increasing L_d, thereby satisfying the FI condition. Although MFB rotor designs have been reported to enable FI operation in IPMSMs [7]-[13], their suitability for high-speed operation is often constrained by reduced mechanical strength resulting from excessive material removal. Moreover, an excessive number of FBs can distort the air-gap flux distribution, leading to non-sinusoidal back electromotive force (EMF), increased torque pulsation, and degraded acoustic performance.

In this context, a systematic investigation of how FBs shape magnetic flux distribution and torque characteristics is essential to realizing the FI effect in SIPM motors without compromising mechanical integrity or electromagnetic performance. This paper examines the application of the FI principle to SIPM motors by incorporating multiple FBs into the rotor core. Building on a baseline SIPM rotor structure, a main flux barrier (MFB) and additional flux barriers (AFBs) are introduced in a controlled manner. The influence of these barriers on electromagnetic performance-including PM flux density, air-gap flux distribution, *d*- and *q*-axis inductances, cogging torque, and output torque under both no-load and load conditions-is systematically analyzed.

The rest of this paper is organized as follows. Section II introduces the FI principle for SIPM motors and presents the associated mathematical models. Section III provides a comparative analysis of the effects of multiple FBs on magnetic flux distribution, inductance characteristics, and torque performance. Section IV discusses the key findings and design insights derived from the analysis. Section V concludes the paper. All results are validated using finite element analysis (FEA).

2. THEORETICAL BACKGROUND AND INVESTIGATION MODELS

2.1. Theoretical Background

Fig. 1 illustrates the torque component distribution in interior permanent magnet synchronous motors (IPMSMs). To establish the theoretical basis for the analysis, the electromagnetic torque of an IPMSM can be expressed as:

$$T_e = \frac{3P}{2}\lambda_m I_q + \frac{3P}{2}(L_d - L_q)I_d I_q \qquad (1)$$

where P is the motor pole pairs, λ_m is the PM flux linkage, I_q and I_d are the currents of the d and q-axes, and L_d and L_q are the inductances of the d and q-axes.

To quantify torque pulsation, the torque ripple is defined as:

$$T_{ripple} = \frac{T_{max} - T_{min}}{T_{max}} 100\% \qquad (2)$$

where T_{max} and T_{min} denote the maximum and minimum torque values, respectively.

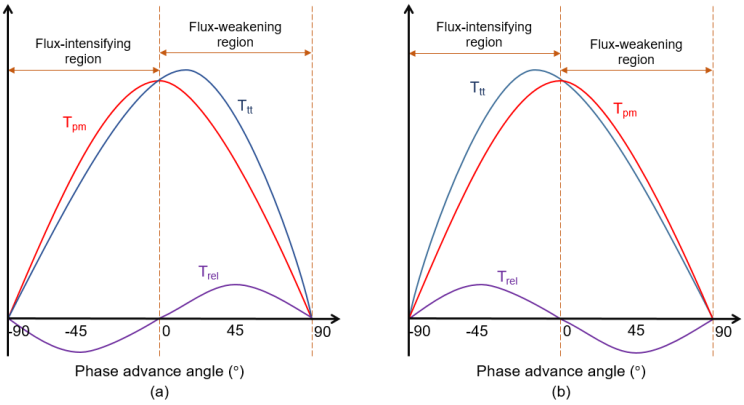

Fig. 1. Torque component distribution in IPMSMs: (a) conventional field-weakening (FW)–based IPMSM with $L_d < L_q$; (b) flux-intensifying (FI)–based IPMSM with $L_d > L_q$.

As shown in Fig. 1, the electromagnetic torque of an IPMSM can be decomposed into permanent magnet torque (T_{PM}) and reluctance torque (T_{rel}). Under normal operation, the q-axis current i_q remains positive, so the PM torque always acts as the driving torque. By contrast, the reluctance torque depends on both inductance characteristics and the current vector orientation, and it can act as either a driving or a braking torque.

To characterize the saliency of the investigated models under different load conditions, the saliency ratio is defined as:

$$\begin{cases} Saliency_{FW-based\ IPMSM} = \dfrac{L_q}{L_d} \\ Saliency_{FI-based\ IPMSM} = \dfrac{L_d}{L_q} \end{cases} \qquad (3)$$

Compared with conventional IPMSMs, the condition $L_d > L_q$, corresponding to FI operation, produces a reverse-salient rotor structure and fundamentally changes the role of reluctance torque. In conventional FW-based IPMSMs with $L_d < L_q$, the reluctance torque acts as a braking torque at negative phase advance angles and as a driving torque at positive phase advance angles. As a result, the maximum total torque (T_{tt}) is obtained at a positive phase advance angle. By contrast, in FI-based IPMSMs with $L_d > L_q$, the reluctance torque becomes positive at negative phase-advance angles, so the maximum total torque is obtained at a negative phase-advance angle.

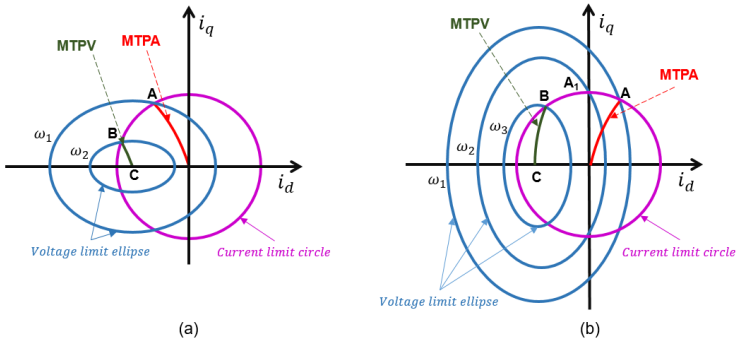

Fig. 2. Current vector trajectories of IPMSMs in the i_d–i_q plane showing MTPA, field-weakening, and MTPV operating regions: (a) FW-based IPMSM; (b) FI-based IPMSM.

The corresponding current-vector trajectories in the i_d–i_q plane are shown in Fig. 2, including the maximum-torque-per-ampere (MTPA), field-weakening (FW), and maximum-torque-per-voltage (MTPV) operating regions. Since $L_d > L_q$, a positive d-axis current ($i_d > 0$) can be applied in FI-based IPMSMs at or below rated speed to enhance PM flux and exploit reluctance torque. Consequently, the MTPA trajectory lies in the first quadrant of the i_d–i_q plane. As speed increases, the current vector follows the MTPA trajectory until the voltage limit is reached, after which i_d gradually decreases to zero. Beyond this point, the machine enters the FW region with $i_d < 0$, followed by the MTPV region at higher speeds. When the current limit is lower than the characteristic current, the machine operates only in the MTPA and FW regions. Therefore, unlike conventional FW-based IPMSMs, where i_d is always negative, FI-based IPMSMs operate with positive i_d at low speeds and negative i_d only at high speeds, thereby enabling a wider constant power speed range (CPSR).

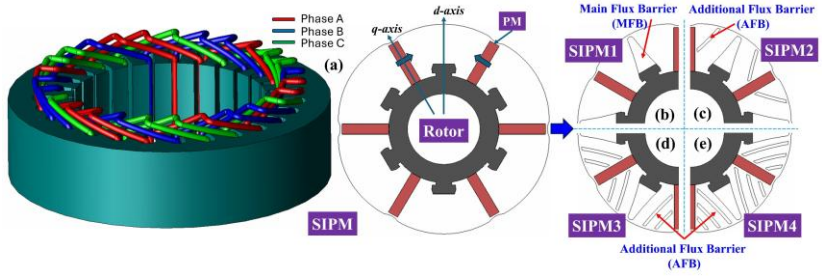

Fig. 3. Model of the 5-kW SIPM motor investigated in this study:
(a) stator winding and baseline rotor configuration; (b) SIPM1 with a main flux barrier (MFB);
(c) SIPM2 with MFB and a one-layer additional FB (1-layer AFB);
(d) SIPM3 with MFB and two-layer additional FBs (2-layer AFBs);
and (e) SIPM4 with MFB and three-layer additional FBs (3-layer AFBs).

2.2. Investigation Models

A 5-kW SIPM motor is selected as the benchmark for this study, as illustrated in Fig. 3. For a fair comparison, the stator configuration is identical across all investigated models and employs a double-layer distributed winding with 27 slots and 6 poles, as shown in Fig. 3(a). This slot–pole combination yields a winding factor of 0.945.

To examine how multiple FBs affect FI operation, a main flux barrier (MFB) and additional flux barriers (AFBs) are added to the rotor core of the SIPM motor. As shown in Fig. 3(b), the MFB is positioned between adjacent poles to create the SIPM1 configuration. Then, AFBs are layered into SIPM1, resulting in the following configurations: SIPM2 with a single-layer AFB (Fig. 3(c)), SIPM3 with two-layer AFBs (Fig. 3(d)), and SIPM4 with three-layer AFBs (Fig. 3(e)). All models are designed to ensure mechanical stability with a safety factor greater than 2.5 [14] and share the same rotor outer diameter, inner diameter, and permanent magnet volume to isolate the electromagnetic effects of the FBs, as summarized in Table 1. The spacing between adjacent FBs is determined based on the available pole area to ensure adequate equivalent flux density and prevent excessive flux crowding.

The primary design objective of introducing *q*-axis FBs is to achieve the FI effect by increasing the *d*-axis inductance and reducing the *q*-axis inductance. However, these modifications significantly alter the rotor flux distribution, making it challenging to preserve the torque characteristics of a conventional SIPM motor. To address this issue, the role of each FB is examined by introducing the barriers in a stepwise manner to decouple their individual and combined effects. This approach enables a systematic assessment of how progressive FB layering influences torque performance and magnetic flux density distribution.

Table 1. Main specifications of motors

Parameter	Unit	Value
Stator diameter	mm	160
Rotor diameter	mm	90.8
Airgap	mm	0.4
Stack length	mm	40
Nominal voltage	V	80
Peak torque	Nm	20.5
Peak Power	kW	5
Base speed	rpm	2000
Maximum Speed	rpm	7000
Stator/Rotor materials		35CS250
Coil pitch		4

3. ANALYSIS RESULTS

3.1. Effect of Multiple FBs on the PM Flux Enhancement

Fig. 4 compares the magnetic flux behavior of five SIPM motor configurations with different numbers of FBs under both open-circuit and on-load conditions. In open-circuit operation, as shown in Fig. 4(a), adding multiple FBs significantly changes the flux paths, guiding magnetic flux more effectively toward the stator teeth and reducing air-gap leakage. As the number of FBs increases from SIPM to SIPM4, the flux lines become more

concentrated and symmetrically distributed, indicating improved magnet utilization and stronger excitation capability.

Under on-load conditions, Fig. 4(b) shows that multi FB configurations (SIPM2–SIPM4) exhibit a more uniform flux density distribution within the stator yoke and rotor core. In contrast, the conventional SIPM shows localized saturation near the magnet edges. This suggests that multiple FBs promote flux redistribution, alleviating local saturation and thereby improving torque-producing capability under load conditions.

Fig. 4(c) further shows the PM flux density within the magnet regions at 105A and a magnet temperature of 120°C. SIPM3 and SIPM4 exhibit higher and more evenly distributed PM flux density compared to configurations with fewer barriers. This enhancement results from improved magnetic coupling between the PMs and the stator, achieved through the optimized FB design. Overall, the findings indicate that adding multiple FBs increases PM flux linkage, lowers the risk of demagnetization, and enhances electromagnetic performance.

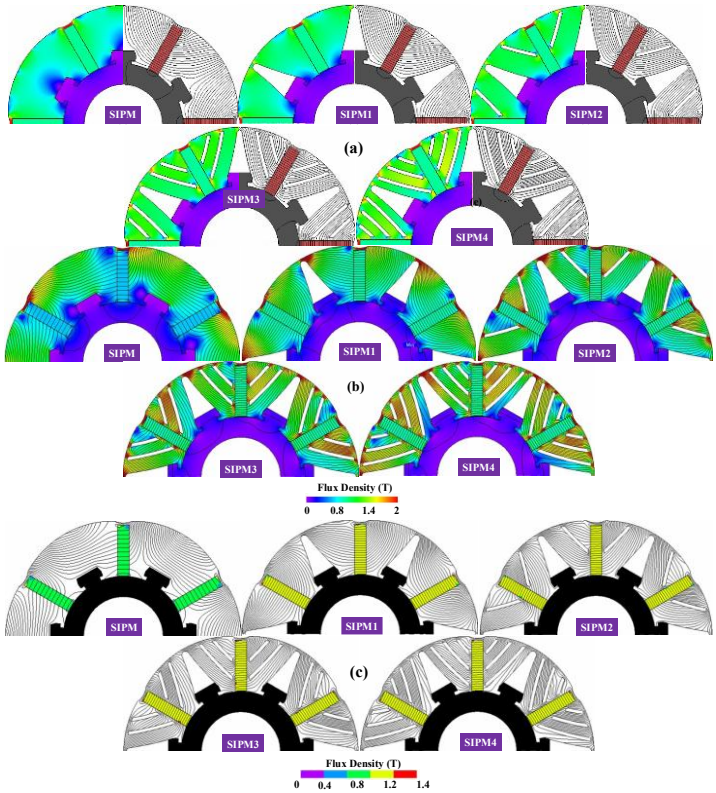

Fig.4. Comparison of magnetic flux density and flux-line distributions for five SIPM motors with different FB configurations: (a) open-circuit; (b) on-load; and (c) PM flux density within the magnets at 120°C.

Fig. 5 evaluates the demagnetization withstand capability of five SIPM topologies under maximum torque per ampere (MTPA) operation, during which armature reaction introduces a strong demagnetizing component in the PM region. As shown in Fig. 5(a), the flux density distribution identifies the most critical PM region, defined as the observation point, where irreversible demagnetization is most likely to initiate.

Compared with the baseline SIPM, the multi FB configurations (SIPM1–SIPM4) exhibit higher flux density in the PM-adjacent region, indicating a reduced effective demagnetizing field acting on the magnets. Figs. 5(b) and 5(c) provide a quantitative comparison at the observation point. As illustrated in Fig. 5(b), the baseline SIPM shows significantly lower flux

density across the electrical rotor position range, implying a smaller demagnetization safety margin under worst-case current conditions. In contrast, SIPM1–SIPM4 maintain higher and more stable flux density levels, reflecting improved magnetic robustness.

Fig. 5(c) further shows that, with increasing current amplitude, the flux density in the baseline SIPM decreases markedly, whereas the multi FB designs experience only a minor reduction. These results confirm that introducing multiple FBs effectively mitigates the demagnetizing effect of armature reaction, thereby enhancing the demagnetization withstand capability of SIPM motors under high-current MTPA operation.

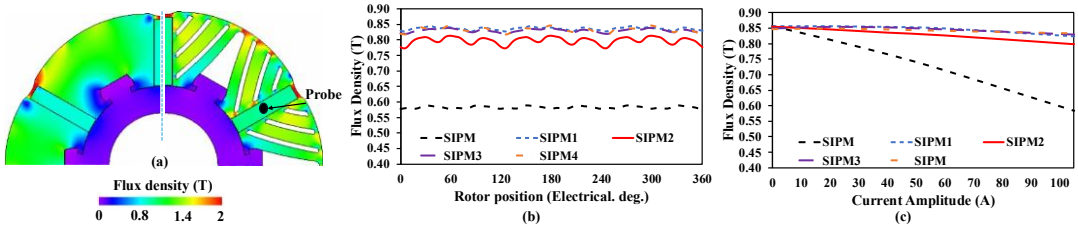

Fig. 5. Demagnetization withstand capability of five SIPM motors under MTPA operation: (a) flux density distribution; (b) flux density at the observation point versus rotor position; and (c) flux density at the observation point versus current amplitude.

3.2. Effect of Multiple FBs on the Flux Linkage, Air-gap Flux Density, and Back EMF

Fig. 6 compares the open-circuit electromagnetic characteristics of the baseline SIPM and the FI designs with multiple FBs (SIPM1–SIPM4). As shown in Fig. 6(a), the back-EMF, air-gap flux density, and flux-linkage waveforms remain largely sinusoidal across all configurations, indicating that the FBs do not significantly distort the fundamental excitation.

As shown in Fig. 6(b), increasing the number of FBs slightly reduces the fundamental back-EMF component, from 32.72 V in the baseline SIPM to 32.17 V in SIPM4, and alters the harmonic spectrum, with higher-order components becoming more pronounced. This behavior reflects changes in the main flux path and leakage flux caused by the barrier geometry. Because no harmonic mitigation techniques are applied, the observed differences are primarily attributed to the FB configuration.

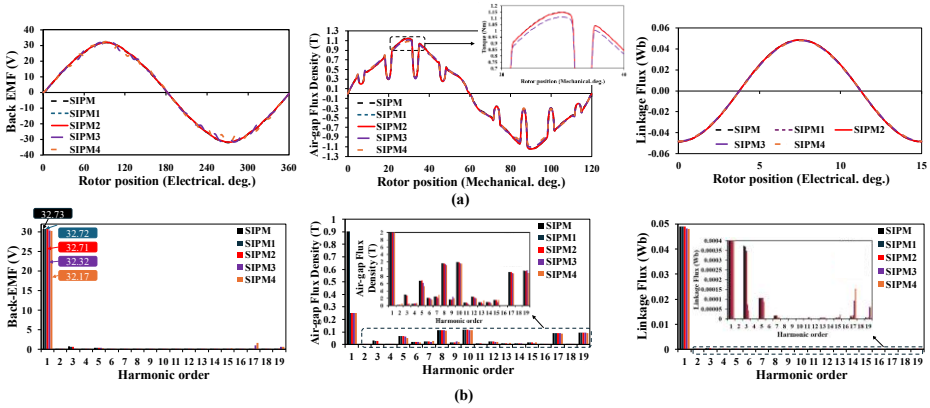

Fig. 6. Comparison of open-circuit electromagnetic quantities for five SIPM motors: (a) back-EMF, air-gap flux density, and flux linkage waveforms; (b) harmonic spectra.

3.3. Effect of Multiple FBs on the Motor Inductances

Fig. 7 shows the variation of the *d*- and *q*-axis inductances and saliency ratios with current amplitude for the five SIPM configurations. As shown in Fig. 7(a), the conventional SIPM exhibits strong current-dependent saturation, leading to sharp reductions in both inductances

and the saliency ratio at high current. In contrast, the multi FB designs in Fig. 7(b)–(e) exhibit improved inductance stability, with L_d increasing slightly and L_q decreasing as current increases, resulting in inverse saliency ($L_d > L_q$). The saliency ratio remains above unity but below approximately 1.35, indicating a moderate anisotropy suitable for FI operation.

3.4. Effect of Multiple FBs on the Torque Characteristics

Fig. 8 compares the open-circuit cogging torque waveforms and harmonic spectra of the investigated motors. The baseline SIPM exhibits the highest cogging torque amplitude (≈0.022 Nm), while the FB designs significantly reduce ripple, with the minimum amplitude of approximately 0.018 Nm observed in SIPM3. Harmonic analysis further shows that higher-order components are progressively suppressed as AFBs are introduced, indicating improved torque uniformity.

Fig. 9 presents the torque–current characteristics under $i_d = 0$ control. All FB configurations produce higher torque than the baseline SIPM, particularly at high current levels. As highlighted in the inset near the rated current, SIPM2 and SIPM4 achieve the highest torque output, demonstrating enhanced FI capability. The approximately linear torque–current relationship confirms good magnetic linearity and efficient current utilization.

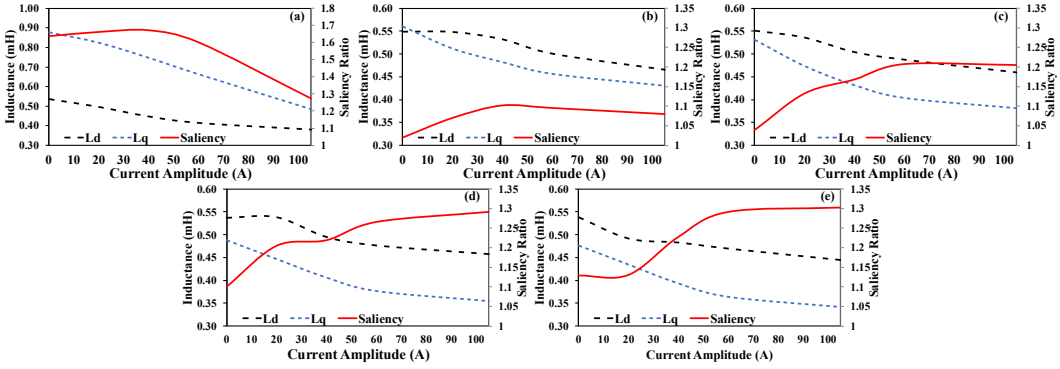

Fig. 7. d- and *q*-axis inductances and saliency ratio versus current for five SIPM motor configurations: (a) SIPM, (b) SIPM1, (c) SIPM2, (d) SIPM3, and (e) SIPM4.

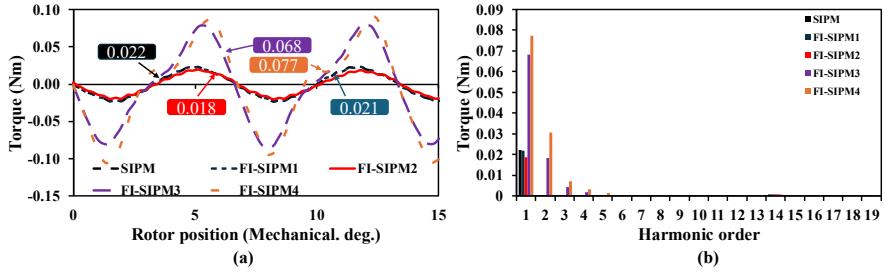

Fig. 8. Comparison of open-circuit cogging torque: (a) Waveforms. (b) Harmonic spectrum.

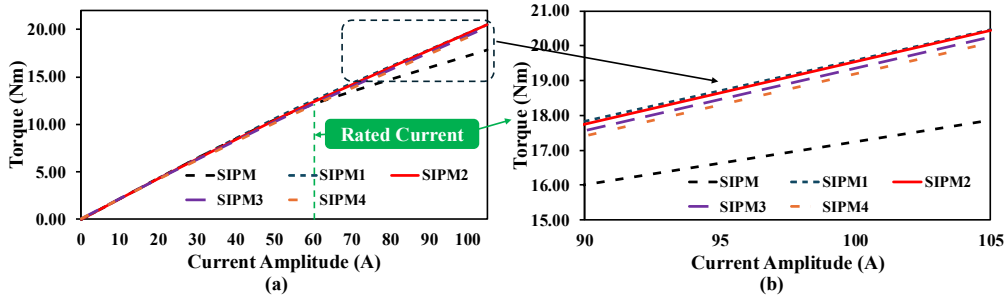

Fig. 9. Output torque of five SIPM motors under $i_d = 0$ control:
(a) torque versus current; (b) an enlarged view of the torque–current characteristics within the specified current range.

Fig. 10 shows the instantaneous torque waveforms at rated current. All multi FB configurations exhibit lower torque ripple than the baseline SIPM. Among them, SIPM3 achieves the lowest torque ripple, approximately 6.1%. This reduction is attributed to the smoother air-gap flux distribution from the multiple FBs, which suppresses local saturation and harmonic torque components.

Fig. 11 compares torque characteristics as a function of current phase angle. For the multi-barrier SIPM designs, the torque peaks shift slightly toward the negative current-angle region, indicating a greater contribution of reluctance torque under FI operation. The maximum torque remains within 20–20.5 Nm for SIPM1–SIPM4, while the optimal current angle varies between −7°E and −10°E. These results confirm that the proposed FB configurations improve *d*-axis flux intensification, leading to smoother torque output and better operating characteristics over a wide current-angle range, as shown in [12].

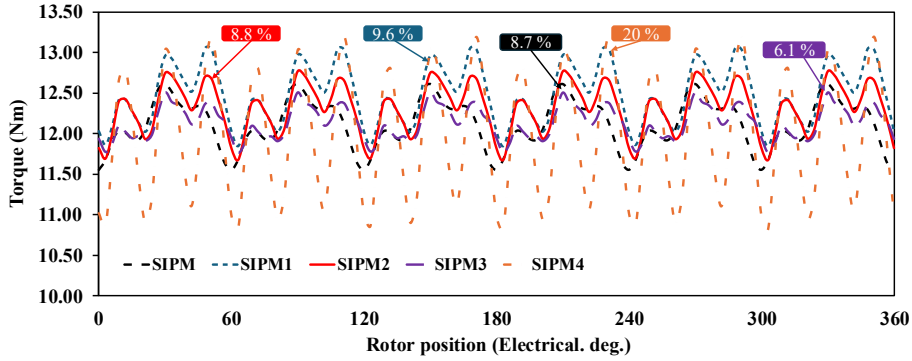

Fig. 10. Output torque waveforms of five SIPM motors at rated current.

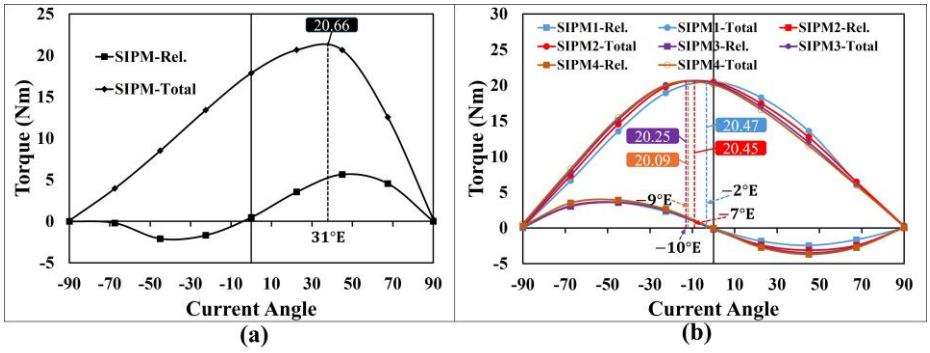

Fig. 11. Output torque and the reluctance torque component of five SIPM motors versus current phase angle: (a) conventional SIPM, (b) proposed SIPM1 to SIPM4.

4. CONCLUSION

This paper examined the impact of multiple FBs on the electromagnetic performance of a 5-kW spoke-type IPMSM, using a conventional SIPM as the baseline. Finite-element results demonstrate that MFBs modify rotor flux paths, increase PM flux utilization, and enhance demagnetization resistance under MTPA operation. The resulting inverse saliency ($L_d > L_q$) allows flux-enhancing operation while maintaining a nearly sinusoidal back-EMF. Overall, the multi-barrier SIPM designs offer higher torque capacity with lower torque ripple, showing

strong potential for EV traction applications that demand robust, high-current, wide-speed operation, a capability that will be explored in future work.

Acknowledgment: The authors would like to thank JSOL, Japan, for supporting JMAG software.

REFERENCES

[1] K. T. Chau, C. C. Chan, and C. Liu, "Overview of permanent-magnet brushless drives for electric and hybrid electric vehicles," *IEEE Trans. Ind. Electron.*, vol. 55, no. 6, pp. 2246–2257, June 2008, doi: https://doi.org/10.1109/TIE.2008.918403

[2] A. Wang, C. Wang, Y. Wang, "Performance Analysis and Comparison of Interior Permanent Magnet Machine with FSCW and Distributed Windings for a Hybrid Electric Vehicle," in *Pro. Int. Conf. Electr. Mach. and Sys. (ICEMS)*, Busan, Korea, Oct. 26-29, 2013, doi: https://doi.org/10.1109/ICEMS.2013.6754400

[3] X. Liu, H. Chen, J. Zhao, and A. Belahcen, "Research on the Performances and Parameters of Interior PMSM Used for Electric Vehicles," *IEEE Trans. Ind. Electron.*, vol. 63, no. 6, pp. 3533-3545, June 2016, doi: https://doi.org/10.1109/TIE.2016.2524415

[4] D. -W. Kang, "Analysis of Vibration and Performance Considering Demagnetization Phenomenon of the Interior Permanent Magnet Motor," *IEEE Trans. Magn.*, vol. 53, no. 11, pp. 1-7, Nov. 2017, doi: https://doi.org/10.1109/TMAG.2017.2708421

[5] K. -Y. Yoon and K. -Y. Hwang, "Optimal Design of Spoke-Type IPM Motor Allowing Irreversible Demagnetization to Minimize PM Weight," *IEEE Access*, vol. 9, pp. 65721-65729, 2021, doi: https://doi.org/10.1109/ACCESS.2021.3070747

[6] D. D. V. Gueter and I. E. Chabu, "Space Vector Flux Weakening in Permanent Magnet Synchronous Machines Considering Demagnetization Risks and its Performance Impacts," in *Proc. IEEE Int. Conf. Ind. Appl. (INDUSCON)*, São Bernardo do Campo, Brazil, 2023, doi: https://doi.org/10.1109/INDUSCON58041.2023.10374699

[7] N.Limsuwan, Y. Shibukawa, D. Reigosa, and R. D. Lorenz, "Novel Design of Flux-Intensifying Interior Permanent Magnet Synchronous Machine Suitable for Self-Sensing Control at Very Low Speed and Power Conversion," *IEEE Trans. Ind. Appl.*, vol. 47, no. 5, September/October 2011, doi: https://doi.org/10.1109/TIA.2011.2161534

[8] X. Zhu, J. Huang, L. Quan, Z. Xiang, and B. Shi, "Comprehensive Sensitivity Analysis and Multiobjective Optimization Research of Permanent Magnet Flux-Intensifying Motors," *IEEE Trans. Ind. Electron.*, vol. 66, no. 4, pp. 2613- 2627, April 2019, doi: https://doi.org/10.1109/TIE.2018.2849961

[9] X. Zhu, W. Wu, S. Yang, Z. Xiang, and L. Quan, "Comparative Design and Analysis of a New Type of Flux-Intensifying Interior Permanent Magnet Motors with Different *q*-axis Rotor Flux Barriers," *IEEE Trans. Energy Convers.*, vol. 33, no. 4, pp. 2260 – 2269, December 2018, doi: https://doi.org/10.1109/TEC.2018.2837119

[10] N. Limsuwan, T. Fukushige, K. Akatsu, R. D. Lorenz, "Design methodology for variable-flux, flux-intensifying interior permanent magnet machines for an electric-vehicle-class inverter rating," in *Pro. IEEE Energy Convers. Cong. and Exp. (ECCE)*, Denver, USA, 2013, doi: https://doi.org/10.1109/ECCE.2013.6646889

[11] D. -K. Ngo, M. -F. Hsieh and T. A. Huynh, "Torque Enhancement for a Novel Flux Intensifying PMa-SynRM Using Surface-Inset Permanent Magnet," *IEEE Trans. Magn.*, vol. 55, no. 7, pp. 1-8, July 2019, doi: https://doi.org/10.1109/TMAG.2019.2897022

[12] V. -V. Do, T. A. Huynh and M. -F. Hsieh, "Design and Analysis of Flux-Intensifying Spoke-type IPM Motor for Improving Output Torque and Flux-Weakening

Performance," in *Pro. Int. Conf. Electr. Mach. and Sys. (ICEMS)*, Chiang Mai, Thailand, 2022, doi: https://doi.org/10.1109/ICEMS56177.2022.9983195

[13] T. A. Huynh, Y. -T. Nguyen Le, Z. Lee, M. -C. Tsai, P. -W. Huang and M. -F. Hsieh, "Influence of Flux Barriers and Permanent Magnet Arrangements on Performance of High-Speed Flux-Intensifying IPM Motor," *IEEE Trans. Magn.*, vol. 59, no. 11, pp. 1-6, Nov. 2023, doi: https://doi.org/10.1109/TMAG.2023.3290538

[14] M.-F. Hsieh, A. T. Huynh, V.-V. Do, D. Gerada, C. Gerada, "Design Optimization of Spoke-type Flux-intensifying PM Motor with Asymmetric Rotor Configuration for Improved Performance," *IEEE Trans. Magn.*, vol. 60, no. 9, pp. 1-5, Jul. 2024, doi: https://doi.org/10.1109/TMAG.2024.3428416